Towards a laser warning system in the visible spectrum using a neuromorphic camera

Orth, Antony; Stewart, Terrence; Picard, Michel; Drouin, Marc-Antoine

Publisher's version / Version de l'éditeur:
https://doi.org/10.1145/3546790.3546819
Proceedings of the International Conference on Neuromorphic Systems 2022, pp. 1-4, 2022-07-27

Towards a Laser Warning System in the Visible Spectrum using a Neuromorphic Camera

Antony Orth[1] Terrence C. Stewart[1], Michel Picard[1] Marc-Antoine Drouin[1]
[1]National Research Council Canada
Ottawa, Ontario, Canada
FirstName.LastName@nrc-cnrc.gc.ca

ABSTRACT

We present an assessment of the use of a neuromorphic camera in a Laser Warning Systems (LWS). The tested configuration is composed of a fisheye lens mounted onto a neuromorphic camera, yielding hemispherical coverage. We show that the tested configuration can identify the angle of incidence of a laser beam to typically within 0.05°. Our results suggest that, in the visible spectrum, neuromorphic camera would combine the advantage of existing camera-based and photodiode-based LWSs.

CCS CONCEPTS

• **Computing methodologies** → **Object detection**; • **Hardware** → *Biology-related information processing*; • **Computer systems organization** → *Sensor networks*.

KEYWORDS

neuromorphic camera, event camera, laser warning system

ACM Reference Format:
Antony Orth[1] Terrence C. Stewart[1], Michel Picard[1] Marc-Antoine Drouin[1]. 2022. Towards a Laser Warning System in the Visible Spectrum using a Neuromorphic Camera. In *ICONS '22: International Conference on Neuromorphic Systems, July 27–29, 2022.* ACM, New York, NY, USA, 4 pages. https://doi.org/10.1145/3546790.3546819

1 INTRODUCTION

Lasers aimed at aircraft put the safety of pilots, crews and passengers at risk. During a laser incident, the pilot may become distracted or temporarily blinded during critical maneuvers. In Canada, laser attacks on aircraft are serious events that are registered in the Civil Aviation Daily Occurrence Reporting System (CADORS). Between 2000 and 2021, a total of 4826 incidents were recorded [11]. The number of laser incidents in Canada reached a peak in 2015 and has recently started to rise again. In the USA, the number of laser strikes was declining until 2018 and then increased to 9723 incidents in 2021, the highest yearly total recorded to-date[1] . The use of a laser detector, known as laser warning system (LWS), can confirm the moment of the incident, the origin of the laser pointer and potentially the wavelength, intensity, and exposure time. This information can be used for prosecution and for evaluating the risk of eye injury.

LWSs are also widely used in military applications for threat detection [5, 7, 14]. There are many commercial [2, 6, 9] and prototype systems [4, 10, 13] available with a variety of viewing angle resolutions, field-of-view (FOV) coverage and wavelength response . Camera-based LWSs have higher angular resolution than photodiode-based systems due to the larger number of pixels [4]. However, photodiode-based systems are smaller [3, 12] and draw less power. Although a small footprint LWS is likely often desirable, the physical size of the aperture can limit the sensitivity of the overall system. These tradeoffs must be considered in choosing the appropriate LWS for a given application.

Neuromorphic cameras are attractive for use in a LWS because laser attacks are expected to be infrequent events and neuromorphic cameras require processing only when events are registered. This would enable a LWS to be deployed with limited power consumption and a small physical footprint compared to an LWS based on a traditional image sensor. Moreover, for fast moving laser threats, localization with a neuromorphic sensor is not restricted by the frame rate of a synchronous readout camera, which also requires a significant power draw to operate at an elevated refresh rates. A neuromorphic LWS has the potential to combined the best of both worlds - high resolution, high sensitivity laser threat detection with a low power draw.

In this paper, we present the results of experiments conducted using a neuromorphic camera for laser threat detection in the visible spectrum. The tested configuration is composed of a fisheye lens mounted on a neuromorphic camera (DAVIS346, iniVation). We show that this combination provides a hemispherical FOV with angular resolution and typical accuracy on the order of $0.05° - 0.1°$.

2 EXPERIMENTAL

An experimental test bench was built to assess the performance of a neuromorphic camera for laser event detection and localization. A schematic of the system is shown in Fig. 1. The camera (iniVation DAVIS346) was mounted on an automated rotation stage (PI M-060PD) in the path of a collimated laser beam (658nm). The laser beam was collimated from the output of a single mode fiber by a 2-inch diameter 200mm focal length plano-convex lens. The camera is fitted with a fisheye lens (Edmund Optics 62-274) that fills the camera sensor with a circle of diameter approximately equal to the frame height. Thus, the camera observes a full hemisphere field of view (FOV).

The image projected onto the camera sensor is made slightly out of focus by using a c-mount spacer ring between the lens and camera. Because of this defocus, the image of the collimated laser

ICONS '22, ICONS '22, 2022, Virtual Event

ACM ISBN 978-1-4503-9789-6/22/07.
https://doi.org/10.1145/3546790.3546819

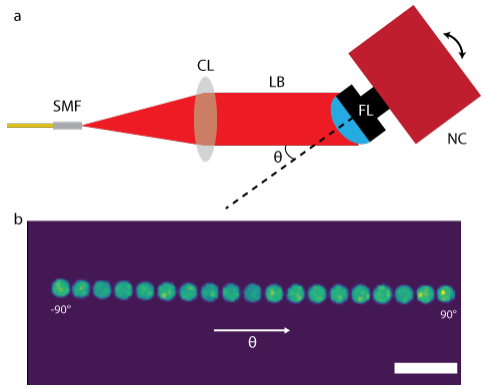

Figure 1: a) Schematic of experimental setup. SMF: Single mode fibre; CL: Collimation lens (200mm focal length); LB: Laser beam (wavelength 658nm); θ: Stage rotation angle; FL: Fisheye lens; NC: Neuromorphic camera. b) Typical event density image acquired when scanning from $-90°$ to $90°$ in $10°$ steps with fisheye lens aperture set to f/4. The frame is cropped vertically. Scalebar is 50 pixels.

beam on the camera sensor is approximately 10 pixels in diameter when the fisheye lens aperture is set to f/4. This defocus is key to being able to precisely localize a light source incident on the lens. If the laser beam were instead imaged in focus, it would span less than a pixel on the sensor. In this situation, localization precision is poor due to the relatively large discretization and low fill factor (22%) of the sensor. However, when imaged with defocus, the event-weighted centroid of the 10 pixel wide spot can be reliably estimated to within a fraction of a pixel diameter.

Our main goal in this work is to assess the capability of the neuromorphic camera with fisheye lens to measure incident angle of a collimated laser beam. Because the collimated laser beam is located at optical infinity, the displacement of the image of a focused spot is expected to vary linearly on the image sensor under the paraxial (small angle) approximation. Although our system is neither paraxial nor in focus, we expect the equidistant design of the fisheye lens to result in an approximately linear displacement vs. angle relationship.

We measure the spot position vs. angle relationship experimentally by acquiring $\Delta T = 4s$ of event data for 10 equally spaced stage rotation angles from $-90°$ to $90°$. The laser beam was set to pulse at 10Hz with a duty cycle of 5%. The time averaged power incident on the fisheye lens was 81nW (all powers reported are for the total power incident on the 50mm diameter fisheye lens). From this 4s event stream for each angle, the event-weighted centroid was calculated. To filter out noise, a morphological opening with a 3x3 square pixel kernel was performed prior to centroid calculation.

In Fig. 2a we show the event-weighted centroid position along the x-axis (the direction of rotation) as a function of stage angle. Although the trend is nearly linear, a linear fit fails to accurately capture the position of the spot at the extremes of the FOV (Fig. 2b). The root-mean-squared error (RMSE) of the linear fit is $0.24°$ when averaged over the $180°$ range of rotation. Although the error of a linear fit is large at the edges of the FOV, the slope of the fit gives

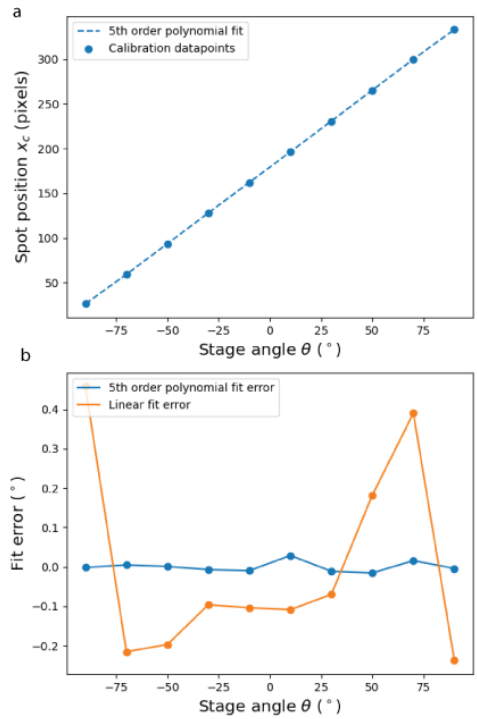

Figure 2: a) Spot position x_c vs. stage angle θ calibration curve. The dashed curve is the 5th-order polynomial fit the the experimental datapoints (circles). b) Fit error for a 5th-order polynomial and a linear fit.

an approximate indication of the angular sampling of the camera and fisheye system: $0.58°/pixel$. To eliminate the systematic errors from a linear calibration, we instead fit a 5th order polynomial to the data:

$$\theta(x_c) = \sum_{n=0}^{5} c_n x_c^n \tag{1}$$

where θ is the stage angle, x_c is the spot centroid position along the x-axis, and the c_n's are fit coefficients. We found that this 5th-order polynomial fit yielded a RMSE of $0.013°$ with roughly uniform magnitude over the FOV (i.e. without large over or under shoots at the edge of the FOV as can be seen in the orange data in Fig. 2b).

3 RESULTS

We assessed the resolution of the neuromorphic laser warning system by measuring the standard deviation of a stationary spot. The laser was set to pulse at 10Hz with 5% duty cycle, and for each pulse the event-weighted centroid was calculated. A typical distribution of the spot centroids (shown in blue) is shown in Fig. 3a for an angle of incidence of $-30°$ and aperture setting of f/4; the mean position of the spot centroids is shown in orange. The same measurement was performed for an angle of incidence ranging from $-90°$ to $0°$ along the horizontal (x) direction. The resulting mean angle from the average centroid $\overline{\Delta\theta}$ is shown as a function of θ is shown in Fig. 3b. Typical values of $\overline{\Delta\theta}$ are between $0.03 - 0.05°$,

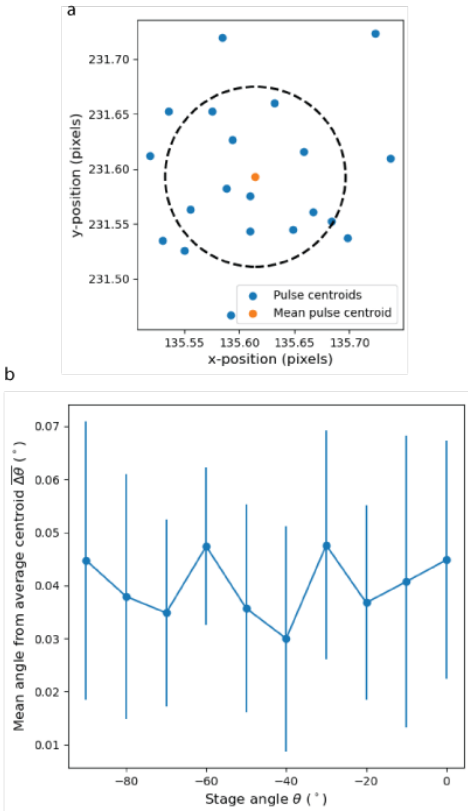

Figure 3: a) Blue spots: laser spot centroids for 20 sequential laser pulses at $-30°$ incidence. Orange spot: mean centroid position. The radius of the dashed black circle is the mean distance from pulse centroids to mean pulse position. b) Mean angle between pulse centroids and mean pulse centroid position (repeatability). Error bars indicate the standard deviation of the angles between the mean pulse centroid and all pulse centroids. These data are all for an aperture setting of $f/4$

$f/\#$	$f/2$	$f/4$	$f/8$	$f/16$
$\overline{\Delta\theta}_{total}$	0.067°	0.040°	0.047°	0.063°

Table 1: Repeatability metric $\overline{\Delta\theta}_{total}$ for apertures $f/2$ - $f/16$

with similar values for standard deviations about this mean. This means the measured angle of incidence of a single 20ms pulse is repeatable to within $0.03 - 0.05°$ with an aperture setting of $f/4$. This repeatability characterization was repeated for different $f/\#$'s; the resulting $\overline{\Delta\theta}_{total}$ values ($\Delta\theta_{total}$ averaged over $-90°$ to $0°$) are presented in Table 1.

From the the data in Table 1, an aperture setting of $f/4$ provides a good tradeoff between spot size and increased signal, with repeatability degrading at either very small or very large aperture settings. Thus, we use $f/4$ for all of the data presented in this paper.

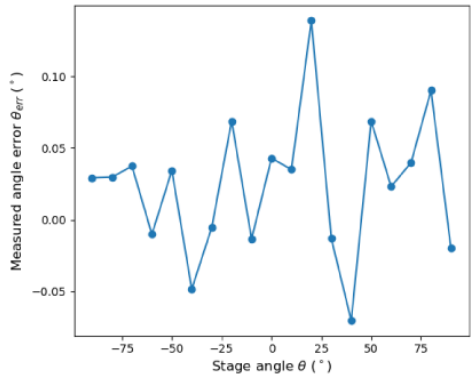

Figure 4: Angle error θ_{err} for an incident laser beam modulated at 80Hz, with duty cycle 50%, with time averaged-power 810nW, integration time 1s.

The accuracy of the neuromorphic LWS was investigated by measuring laser spot positions at varying stage angles across the FOV and comparing with the ground truth angle of incidence given by the stage position (manufacturer's resolution specification: 0.0018°). After finding the centroid position on the image sensor, the measured angle of incidence of the laser θ_{meas} was found via Eq. 1. A typical example of the the difference between the measured angle and the stage angle $\theta_{err} = \theta_{meas} - \theta$ is shown in Fig. 4. For this example, the laser was modulated at 80Hz (duty cycle 50%), with an integration time of 1s. The RMS error (RMSE) of the measured angle of incidence (over all angles) in this case is 0.054°.

This RMSE value depends on the laser modulation frequency due to the high pass filter in the neuromorphic camera circuitry. For all data in this paper, the bias settings were tuned manually to increase responsiveness at high frequencies. In Fig. 5a, (same illumination parameters as for Fig. 4), the RMSE (green dashed curve) initially improves with increasing laser modulation frequency (due to more events per unit time) and then degrades rapidly at 1kHz when the cutoff frequency of the neuromorphic camera's hardware is reached. To illustrate the effect of frequency on the response of the neuromorphic camera, we measured the event frequency response function for incident powers ranging from 20nW to 9631nW, as shown in Fig. 5a. While the event response rate drops sharply at higher frequencies, the value of the cut off frequency increases with increasing power. We define the cutoff frequency as the frequency at which the number of events per pulse drops to 10^{-1}; the resulting cutoff frequencies are plotted in Fig. 5b. At 20nW incident power, repeated pulses are not detectable above 40Hz compared to a cutoff of 4kHz at 9631nW. Above the cutoff, individual pulses are not detectable and instead, the laser appears as a continuous wave (CW) source: the laser is observable only when it is turned on or off. For a quasi-CW source pulsing at 1Hz, we measured a detection limit of 1.2nW of time averaged incident power (0.06nW/cm^2) for a 500ms pulse (2.4nW during the pulse, orange datapoint in Fig. 5b).

4 DISCUSSION AND CONCLUSIONS

In this work we presented the results of our investigation on the use neuromorphic image sensor within LWS. The tested device

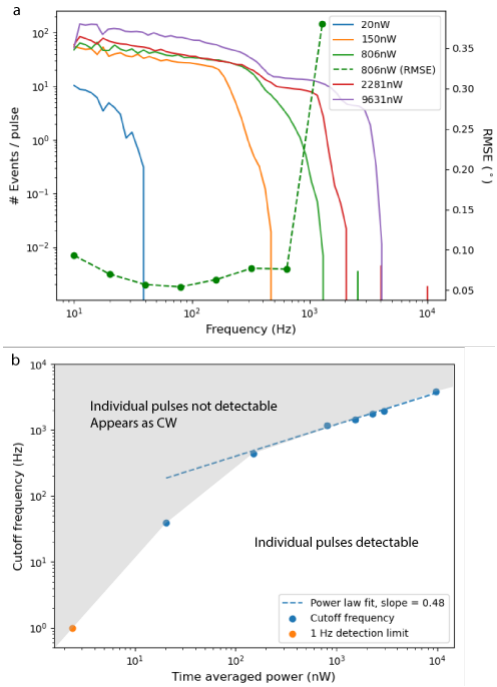

Figure 5: a) Event frequency response function for varying incident laser powers (left y-axis) and RMSE for 806nW incident power (right y-axis). b) Frequency cutoff values where response in (a) drops to 10^{-1}. In the gray region, individual pulses are not visible, and instead a pulse laser will appear as a CW source. The orange datapoint indicates the minimum time-averaged power for which a 1Hz, 50% duty cycle (quasi-CW) pulse is detectable.

consist of a fisheye lens with a hemispherical FOV, mounted with a slight defocus to an iniVation DAVIS346 neuromorphic camera. The position of resulting laser spot is calibrated as a function of incident angle using an automated rotation stage setup. We measured a typical repeatability $\overline{\Delta\theta}_{total}$ of $\approx 0.04-0.07°$, and accuracy (RMSE) of $\approx 0.05-0.1°$.

For most LWS applications, the laser source is expected to be moving with respect to the LWS. Thus, a quickly pulsing laser is newly observable every time a new pixel is irradiated, thereby mitigating the adverse effect of the $\approx 10^3 Hz - 10^4 Hz$ frequency cutoff. Even if the laser spot is stationary on the image sensor, we verified that a quasi-CW (1Hz, 50% duty cycle) source is detectable if the incident energy at the LWS is above 1.2nJ/pulse. A neuromorphic LWS has the potential to combine the advantages of photodiode-based LWSs and camera-based ones. - high resolution, high sensitivity laser threat detection with a low power draw.

The strong frequency dependent response shown in Fig. 5 is a reminder that the ability of neuromorphic cameras to capture fast dynamics is not completely captured by the sensor's timing accuracy or latency metrics. The actual single pixel frequency response ($\approx 10^3 Hz - 10^4 Hz$) is significantly slower than the timing accuracy may suggest $1/1\mu s = 10^6 Hz$. While the single pixel response in Fig. 5 is known [8], most of the recent literature focuses on moving stimuli. We caution against overestimating the capability of neuromorphic cameras to detect fast, spatially stationary stimuli, as may be encountered in other fields.

In future work, the combination of the interleaved event sensing and standard irradiance sensing pixels in the DAVIS346 camera may by leveraged to further increase repeatability, accuracy and detectability for low incident power and/or high pulse frequency scenarios.

ACKNOWLEDGMENTS

This work was supported by the Defence Research and Development Canada and by the National Research Council of Canada. The authors acknowledge F. Théberge for useful discussions.

REFERENCES

[1] Federal Aviation Administration. 2022. Laser Incidents. Internet. https://www.faa.gov/about/initiatives/lasers/laws
[2] Aselan. 2022. LIAS. Internet. https://www.aselsan.com.tr/en/capabilities/electro-optic-systems/air-platforms/lias-laser-warning-receiver-system
[3] Andre Cantin, Jacques Dubois, Paul P. Webb, Daniel Pomerleau, and Michael P. Altman. 1997. Miniaturized digital high-angular-resolution laser irradiation detectors (HARLID) for laser warning receivers (LWR). In *Infrared Technology and Applications XXIII*, Bjorn F. Andresen and Marija Strojnik (Eds.), Vol. 3061. International Society for Optics and Photonics, SPIE, 47 – 57. https://doi.org/10.1117/12.280396
[4] Hongjun Dong and Long Wang. 2012. Non-iterative spot center location algorithm based on Gaussian for fish-eye imaging laser warning system. *Optik* 123, 23 (2012), 2148–2153. https://doi.org/10.1016/j.ijleo.2011.10.012
[5] J. Dubois and F. Reid. 2007. Detecting laser sources on the battlefield. In *Photonics North 2007*, John Armitage (Ed.), Vol. 6796. International Society for Optics and Photonics, SPIE, 747 – 762. https://doi.org/10.1117/12.779234
[6] Excelitas. 2022. EXACTD-362 Angle-of-Arrival Photodiode Module. Internet. https://www.excelitas.com/product/exactd-362-angle-arrival-photodiode-module
[7] Sushil Kumar, Satya Prakash, Anil Maini, V Patil, and Rishi Sharma. 2011. Design of a Laser-Warning System Using an Array of Discrete Photodiodes-Part I. *Journal of Battlefield Technology* 14 (01 2011).
[8] Patrick Lichtsteiner, Christoph Posch, and Tobi Delbruck. 2008. A 128× 128 120 dB 15 μs Latency Asynchronous Temporal Contrast Vision Sensor. *IEEE Journal of Solid-State Circuits* 43, 2 (2008), 566–576. https://doi.org/10.1109/JSSC.2007.914337
[9] Jan Pietrzak. 2003. Laser warning receivers. In *Laser Technology VII: Applications of Lasers*, Wieslaw L. Wolinski, Zdzislaw Jankiewicz, and Ryszard Romaniuk (Eds.), Vol. 5229. International Society for Optics and Photonics, SPIE, 318 – 322. https://doi.org/10.1117/12.520769
[10] Mazhar Tayel, Mohamed Shehata, and Amir Almslmany. 2018. A New Advanced Design and Implementation of Laser Warning System. In *2018 13th International Conference on Computer Engineering and Systems (ICCES)*. 219–224. https://doi.org/10.1109/ICCES.2018.8639218
[11] transport Canada. 2022. The Civil Aviation Daily Occurrence Reporting System (CADORS). Internet. https://tc.canada.ca/en/aviation/publications/aviation-safety-letter/issue-2-2021/civil-aviation-daily-occurrence-reporting-system-cadors
[12] Paul P. Webb, Steven M. Soltesz, Andre Cantin, Jean Fortin, and Daniel Pomerleau. 2001. Improved miniaturized HARLID for laser warning systems having high angular resolution. In *Infrared Technology and Applications XXVII*, Bjorn F. Andresen, Gabor F. Fulop, and Marija Strojnik (Eds.), Vol. 4369. International Society for Optics and Photonics, SPIE, 194 – 200. https://doi.org/10.1117/12.445288
[13] Jacek Wojtanowski, Marcin Jakubaszek, and Marek Zygmunt. 2020. Freeform Mirror Design for Novel Laser Warning Receivers and Laser Angle of Incidence Sensors. *Sensors* 20, 9 (2020). https://doi.org/10.3390/s20092569
[14] Marek Zygmunt and Krzysztof Kopczynski. 2020. Laser warning system as an element of optoelectronic battlefield surveillance. In *Radioelectronic Systems Conference 2019*, Piotr Kaniewski and Jan Matuszewski (Eds.), Vol. 11442. International Society for Optics and Photonics, SPIE, 1 – 7. https://doi.org/10.1117/12.2565139